Available online at www.sciencedirect.com
ScienceDirect
Thin Solid Films 515 (2007) 8386–8392
thin solid films
www.elsevier.com/locate/tsf

# Growth of permanganate conversion coating on 2024-Al alloy

S.A. Kulinich, A.S. Akhtar, P.C. Wong, K.C. Wong, K.A.R. Mitchell *

*Department of Chemistry, University of British Columbia, 2036 Main Mall, Vancouver, BC, Canada V6T 1Z1*

Received 4 August 2006; received in revised form 16 April 2007; accepted 30 April 2007
Available online 22 May 2007

**Abstract**

The growth of permanganate conversion coating on aluminum 2024-T3 alloy has been studied by characterizing, with scanning Auger microscopy, scanning electron microscopy, X-ray photoelectron spectroscopy (XPS) and energy-dispersive X-ray spectroscopy, the coatings formed by immersion of the alloy in the coating bath (containing $KMnO_4$ and $Na_2B_4O_7$, pH 9.1) for different periods of time and at different temperatures. At room temperature, during the first 1–5 min of immersion, $MnO_2$ deposits are formed only on the second-phase intermetallic particles (of Al–Cu–Mg and Al–Cu–Fe–Mn types), but the coating starts to develop on the Al matrix surface after 5–10 min. The coating slows down and stops after about 150 min, with a thinner deposit over the alloy matrix. The process is accelerated at higher temperatures, for example at 68 °C it self-limits after about 3 min. The electrochemical growth process appears to follow that established for the chromate conversion coatings, although XPS does not detect significant $MnO_4^-$ incorporation into the permanganate coatings.
© 2007 Elsevier B.V. All rights reserved.

*PACs:* 81.65.Kn; 81.05.Bx; 68.37.Xy
*Keywords:* Permanganate conversion coating; Aluminum alloy; Surface microstructure; Auger spectroscopy; XPS; SEM; EDX

## 1. Introduction

Conversion coatings are applied to aluminum alloys to improve corrosion resistance and the adhesion of organic paints. Chromate conversion coatings (CCCs) have been applied widely for several decades, but health concerns associated with them are stimulating the development of more environmentally-friendly treatments [1–5]. One alternative approach is provided by permanganate conversion coatings (PCCs) which are reported to give comparable protective properties, but without the deleterious environmental effects of the CCCs [6–11].

The PCC system is based on Mn(VII) in solution being reduced to oxide of lower oxidation state which coats and passivates the substrate analogously to the CCC process [6,8], where chromates are reduced to Cr(III) oxide/hydroxide, along with metallic oxidation. Similar to CCCs, the PCC process is reported to be self-limiting, and does not continue beyond the formation of a thin yellow-gold film [8]. After drying, the PCC-coated metal is usually painted, and there are reports of favorable properties, such as for paint adhesion and filiform corrosion protection [7–11].

However, there are some differences between the CCC and PCC systems. While the CCC process gives a protective inorganic polymer, the PCC system does not, which makes it less affected by heat, and gives fewer restrictions for painting compared with the CCCs [8,12]. For many Al alloys, PCCs and CCCs are reported to provide similar levels of corrosion protection [8–11], but the former work less well for the Cu and Zn-rich alloys (2XXX and 7XXX series), where use of an organic seal is needed after a PCC treatment in order to increase the corrosion resistance sufficiently. In the context of Mg alloys, PCCs have also been reported to give similar corrosion resistance to the CCCs [13–17], and another development is based on a permanganate-phosphate treatment [18,19].

Although PCCs appear to have some promising properties as possible alternatives to CCCs on Al alloys [6–8], information on these coatings is limited and often restricted to patent claims [9–11,20]. While Danilidis et al. [6] described PCCs grown by a 'no-rinse' procedure on AA3003 alloy, and Bibber has reported promising anticorrosive performances for PCCs on various Al alloys [7–11], the formation and growth mechanisms of such coatings are still unknown. That issue is investigated in this

* Corresponding author. Tel.: +1 604 822 5831; fax: +1 604 822 2847.
*E-mail address:* karm@chem.ubc.ca (K.A.R. Mitchell).

0040-6090/$ - see front matter © 2007 Elsevier B.V. All rights reserved.
doi:10.1016/j.tsf.2007.04.164

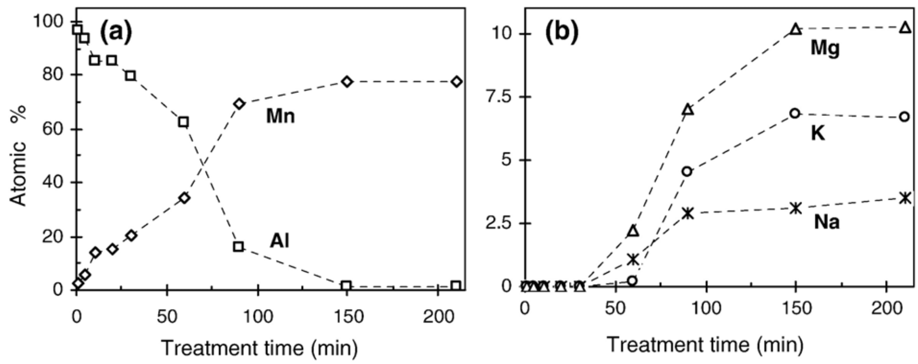


Fig. 1. Relative amounts from XPS of major (a) and minor (b) metallic components in the surface layer of growing PCCs as a function of treatment time at 25 °C. The dashed lines are given to guide the eye.

research which depends on using scanning Auger microscopy, X-ray photoelectron spectroscopy (XPS), scanning electron microscopy (SEM) and energy-dispersive X-ray (EDX) spectroscopy to follow both early and later growth stages of PCCs over the AA2024-T3 aluminum alloy, used in aerospace applications (henceforward this alloy is abbreviated as 2024-Al). Special attention was paid to early growth over the intermetallic second-phase particles of types Al–Cu–Mg and Al–Cu–Fe–Mn [21], as well as on the alloy matrix.

This work aims to clarify two issues with regard to PCC formation on a sample of 2024-Al alloy. The first is how the PCCs nucleate and grow with respect to the alloy microstructure. The second issue concerns whether Mn(VII) species incorporate into the growing conversion films, a topic of relevance to the so-called 'self-healing' of damaged coatings [1,3,4,12].

## 2. Experimental details

Prior to coating, the 2024-Al plates (1 x 1 $cm^2$) were mechanically polished to a mirror finish, degreased successively in acetone and methanol, both in an ultrasonic bath, and finally dried in air. The freshly-polished samples were coated by immersion in a solution containing 0.1 M $KMnO_4$ and 0.05 M $Na_2B_4O_7 \cdot 10\ H_2O$ (borax) at 25 °C for periods ranging from 1 to 210 min. The bath recipe used is among those proposed by Bibber [9–11], and the concentration of $KMnO_4$ is close to that used by Danilidis et al. [6]. During the treatment, the solution was stirred and the samples were suspended vertically in the bath. Because of previous interest in the effect of temperature [7–11], two additional samples were prepared by coating for 3 min at 50 °C in one case and at 68 °C in the other. As a final step, each coated sample was washed in distilled water and dried in air.

The scanning Auger microscopic analysis was conducted with a Microlab 350 spectrometer (Thermo Electron Corp.) with field emission source and hemispherical energy analyzer. Point analysis was carried out using the primary electron beam set at 10 keV and 4 nA; composition analysis was accomplished using the Avantage software provided by the manufacturer. A Hitachi S-3000 N microscope with the incident beam accelerated through 5–20 kV was used for the EDX and SEM analyses. Each EDX spectrum was acquired over a collection time of 100 s. The relative amounts of different elements were determined using the standardless method [22]. The XPS measurements were made with a Leybold MAX200 spectrometer using the Al Kα source (1486.6 eV) operated at 15 kV and 20 mA. All binding energies were corrected for sample charging by referencing to the adventitious hydrocarbon peak in the C 1s spectrum at 285.0 eV.

## 3. Results and discussion

### 3.1. Coating chemical composition

XPS spectra of the samples were collected in order to assess how the surface chemical composition, to within the probe depth of the technique (≤ 10 nm), changes with time. The evolution of the metallic elements detected by XPS for permanganating times from 1 to 210 min is shown in Fig. 1. The dominant metallic component over time is Mn, as expected from previous reports [6], and the amount of Al detected steadily decreases as the substrate is covered. For coating at 25 °C, the underlying Al is no longer recognized after about 150 min. However, for coating times greater than 50 min, there is clear evidence for $Mg^{2+}$, $K^+$ and $Na^+$ being incorporated into the growing PCCs (Fig. 1b). In addition, samples coated for 1–5 min demonstrated trace amounts of Cu in their XPS spectra. Since Cu was not detected for immersions longer than 5 min, we assume that these peaks at the early growth stage were mainly from the 2024-Al substrate (including the substrate-coating interface), and that no significant amount of Cu was incorporated into the coating at the later stages of growth. No B, originating from the borate in the solution, was detected in the coating by XPS.

Quantitative analyses of the XPS spectra for samples PCC treated for 3 min at 50 °C and at 68 °C demonstrated surface compositions similar to those samples prepared at 25 °C for 90 and 210 min respectively. Morphologically, the samples prepared at elevated temperatures were also similar to those prepared at room temperature with the immersion times mentioned. These trends are broadly similar to observations

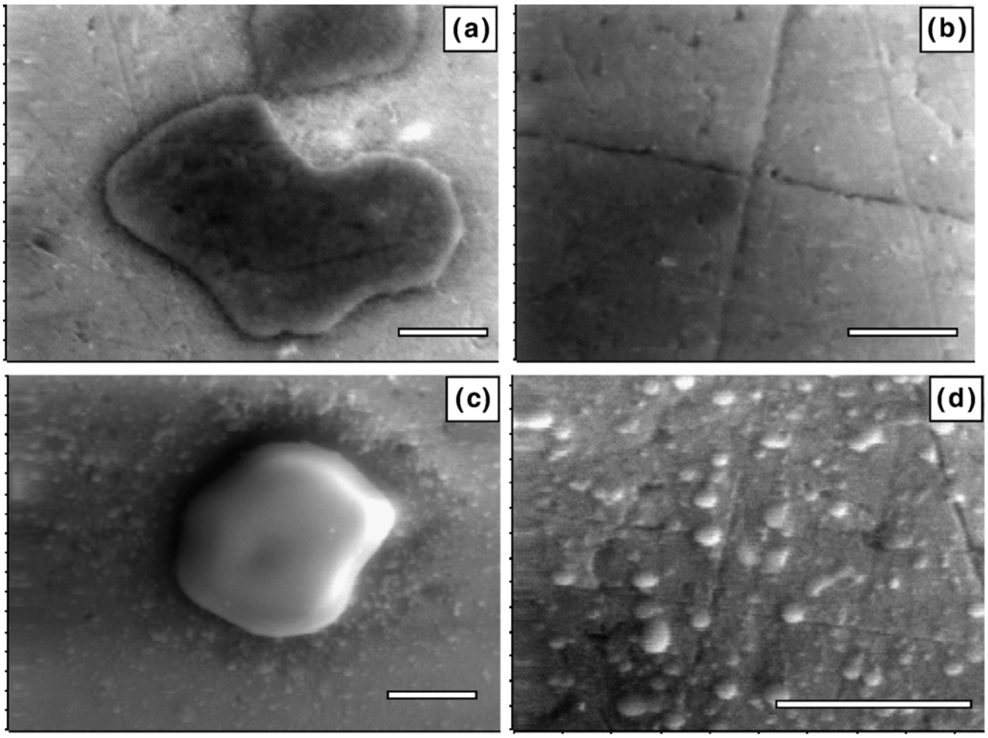


Fig. 2. SEM images from different regions of 2024-Al samples after PCC-treatment at 25 °C for different coating times: (a) both types of second-phase particle after 1 min; (b) alloy matrix after 1 min; (c) Al–Cu–Mg particle after 20 min; (d) alloy matrix after 20 min. Each scale bar indicates 2 μm.

for temperature effects made by Bibber [9], who reported that PCCs with similar properties can be prepared by immersing Al alloys into basic $KMnO_4$ for 1 min at 68 °C, 1.5–2 min at 57–63 °C, or for ~ 60 min at 25 °C.

According to the Pourbaix diagram for Al [23,24], the surface oxide is unstable at the pH used (~ 9.1), and its etching is expected to follow:

$$Al_2O_3 + 2OH^- + 3H_2O \rightarrow 2Al(OH)_4^-. \quad (1)$$

Then reactions at the freshly exposed Al surface can follow the half-reactions:

$$Al + 4OH^- \rightarrow Al(OH)_4^- + 3e^- \quad (2)$$

$$MnO_4^- + 2H_2O + 3e^- \rightarrow MnO_2 + 4OH^-, \quad (3)$$

with the overall formation reaction for PCCs on Al in basic solution given as:

$$Al + MnO_4^- + 2H_2O \rightarrow Al(OH)_4^- + MnO_2. \quad (4)$$

XPS analysis did not detect Al species from the thicker PCCs, implying that any incorporation of aluminate into the coatings must be small (after rinsing).

In principle, when Al is released into solution according to reactions (1) and (4), some alloying elements (e.g. Mg, Cu, Fe and Mn in 2024-Al) could also be released. The only such element that is clearly represented in the coating is Mg but, as noted in Fig. 1b, K and Na, from the permanganating bath, do incorporate at the later stages of the coating process.

### 3.2. Early stages of coating growth

Fig. 2 shows examples of SEM images of 2024-Al samples which have been permanganate treated at 25 °C for different periods of time: 1 min (a,b) and 20 min (c,d). The discussion focuses on three main types of microstructural region, namely the alloy matrix and the Al–Cu–Mg and Al–Cu–Fe–Mn second-phase (intermetallic) particles. While the alloy matrix of 2024-Al still demonstrates polishing scratches, and thus looks etched rather than coated after 1 min of the permanganate immersion (Fig. 2b), the intermetallic particles in Fig. 2a look relatively intact and topographically pronounced compared with the surrounding alloy matrix. This could result either from a slower etching of the particles or from a greater deposition on them within this time of treatment.

After the 20 min treatment, the intermetallic particles (e.g. Fig. 2c) appear even more topographically pronounced, thus supporting the idea that further deposition has occurred over them, and the observed "zones of influence" [25] around some particles is a signature of their electrochemical activity. For instance, the zone extending for ~ 2 μm from the particle in Fig. 2c is likely a result of more intense electrochemical processes, including etching and deposition, in the vicinity of the particle caused by its cathodicity and much smaller size relative to the surrounding matrix. At the same time, the Al matrix also shows change in the sense that the polishing

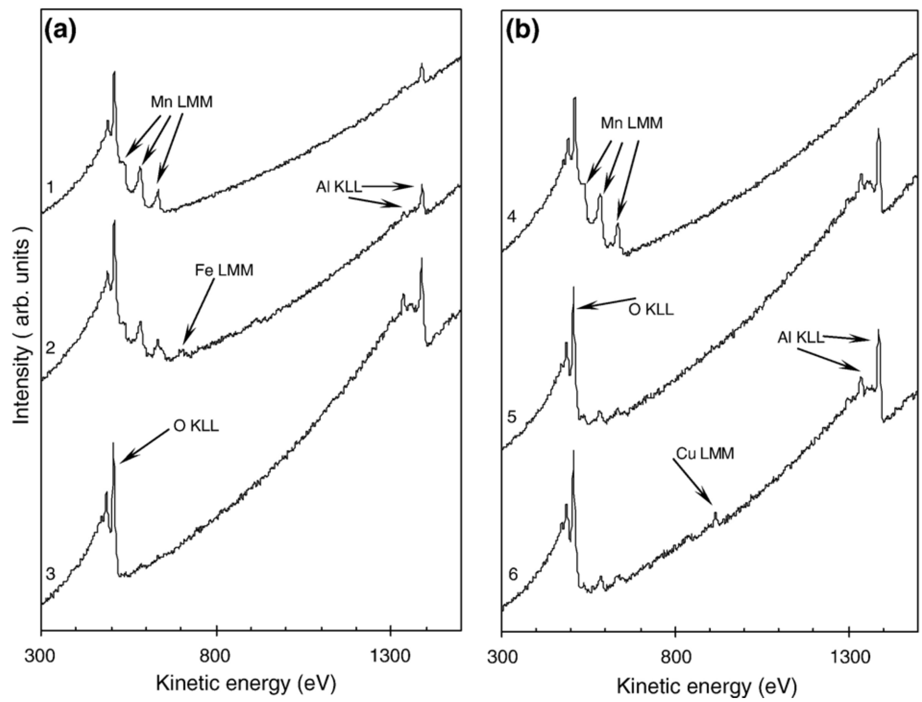


Fig. 3. Auger point spectra measured from 2024-Al samples after PCC-treatment at 25 °C for different coating times. (a) 1 min: (1) Al–Cu–Mg particle, (2) Al–Cu–Fe–Mn particle, (3) alloy matrix; (b) 5 min: (4) Al–Cu–Fe–Mn particle, (5) alloy matrix well removed from intermetallic particles, and (6) alloy matrix close to an Al–Cu–Fe–Mn particle. The arrows identify the most intense peaks in the elemental KLL or LMM series.

scratches have become less dominant, and hillock-like islands (most likely deposits) occur in Fig. 2d. The topography of the PCC over the alloy matrix after 20 min treatment (round hillock-like structures) is consistent with that reported by Danilidis et al. for their PCC prepared by a 'no-rinse' procedure [6]. No obvious particle dealloying was seen by SEM in this work for the samples permanganated for 1–20 min and, except for some pits (most likely from loose and mechanically damaged particles), the second-phase particles looked unchanged (with a dense and relatively uniform coating). This is in contrast to CCCs where particle dealloying has been observed [26–29]. The coating bath conditions are less severe for PCCs (pH ∼ 9 compared to ∼ 2 for CCCs), resulting in less dissolution of Mg and Al from the Al–Cu–Mg particles.

Fig. 3 shows some typical Auger spectra collected from different surface locations after the PCC treatment for 1 min (a) and 5 min (b). The spectra in Fig. 3a allow the conclusion that Mn is present over both the Al–Cu–Mg (1) and Al–Cu–Fe–Mn (2) types of second-phase particles, while no Mn is detected over the alloy matrix. This is consistent with conclusions surmised from Fig. 2a,b about topography at the intermetallic particles compared to the matrix. As a weak peak of Fe is observed in spectrum (2) (Fig. 3a), one can conclude that the $MnO_2$ coating thickness on the Al–Cu–Fe–Mn particle is less than 10 nm, which is consistent with the presence of a fairly strong Al signal. Consistently with the above conclusions about relative coating thickness at different microstructural areas, the Al signal in spectrum (3), from the alloy matrix, is strong and much greater than that in spectrum (1) from the Al–Cu–Mg particle, where the coating is thicker.

Although the particles analyzed demonstrated some individuality in coating thickness, the spectra in Fig. 3a demonstrate the inhomogeneous nature of the coating distribution over the 1 min sample: while all former intermetallic particle regions are well covered by PCC, no detectable Mn is seen over the matrix regions. Interestingly, there was no difference between Auger spectra taken from polishing scratches and from the relatively flat regions, implying that surface etching was dominating over all the alloy matrix during the first 1 min of permanganate immersion at 25 °C.

In comparison to those in Fig. 3a, the Auger spectra in Fig. 3b (for a sample after the 5 min immersion) clearly show the initiation of Mn deposition on the Al matrix (spectra (5) and (6)). Spectrum (4) presents a very small Al peak and no structure for Fe, which implies that the PCC over the Al–Cu–Fe–Mn particle is 10 nm or more thick (a similar spectrum, not shown, was measured for the Al–Cu–Mg particle after the 5 min immersion). Spectrum (6) demonstrates that Cu precipitates could be found on the alloy matrix near to the second-phase particles, where a "zone of influence" is established, as demonstrated in Fig. 2c. This implies some particle dissolution, with Cu clusters washed away and reprecipitated, and supports the belief that the electrochemical character of PCC growth on 2024-Al has a somewhat similar mechanism to that for CCC formation on 2024-Al, specifically with respect to preferential deposition on cathodic regions [26–29]. It should be added that cathodic sites on the 2024-Al surface are not only confined to the large second-phase particles; they can also be present on the Al matrix due to heterogeneities, including those associated with alloying

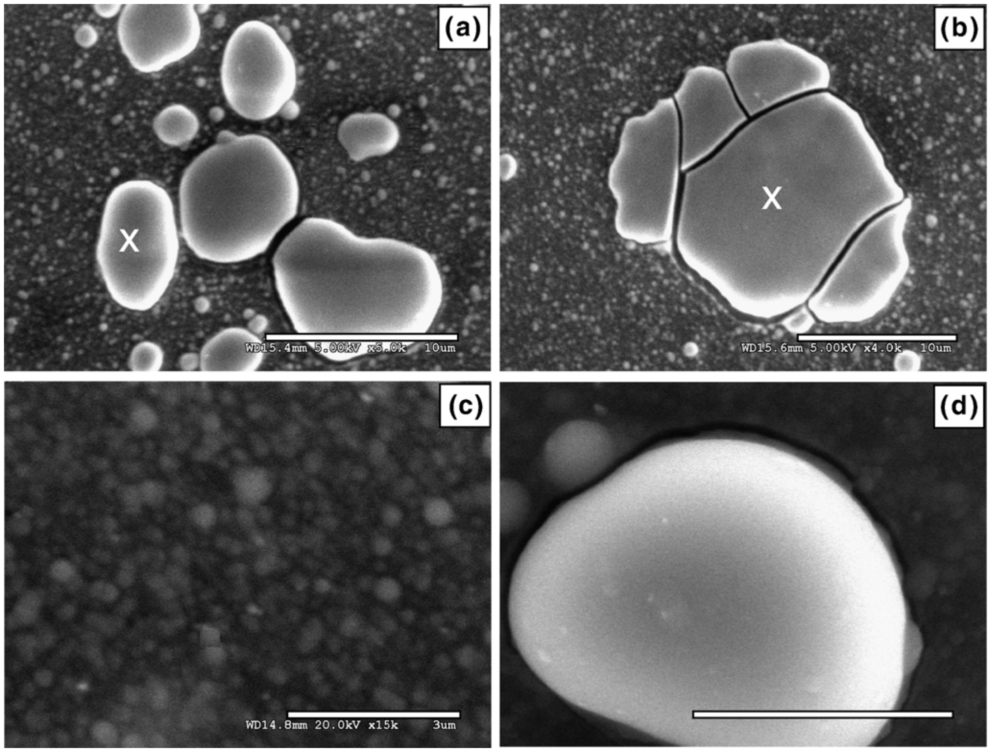


Fig. 4. SEM images from different regions of 2024-Al samples after PCC-treatment at 25 °C for different coating times: (a) cluster of Al–Cu–Mg particles with uniform coating after 90 min; (b) Al–Cu–Fe–Mn particle with cracked coating after 90 min; (c) hillock-like structure on alloy matrix after 150 min; (d) Al–Cu–Mg particle with peripheral trench after 150 min. Scale bars indicate 10 μm for (a,b), 3 μm for (c,d).

elements and intergrain boundaries [26]. Electrochemical activity of such sites could be responsible for PCC deposition over the metal matrix surface.

Auger spectra taken on the Al matrix for samples treated for 10 and 20 min confirm an increase in intensity of Mn signals and hence further growth of the PCC; this supports the assumption stated above based on Fig. 2c,d. Taken all together, this evidence shows the PCC grows on the second-phase particles during the first five minutes, and then nucleates with growth over the alloy matrix especially during the period 5–20 min.

XPS provides more chemical information to supplement the observations from point Auger analysis. The metallic components in Al 2p spectra were only observed for samples immersed for 1 or 5 min. This suggests that the PCC and any Al oxide which may survive after the treatment at 25 °C is thicker than ~ 5–10 nm after the 10 min immersion. Then, in parallel, Cu 2p peaks were seen only for samples PCC treated for 1 and 5 min, the element being presumably from the substrate (intermetallic particles and alloy matrix). At the 10 min treatment, those peaks were no longer detected, so supporting the conclusion that the PCCs continuously covered the substrate, with a thickness (including any remaining Al oxide) of greater than ~ 10 nm.

The above observations for the initial growth of PCC with respect to the substrate microstructure suggest a mechanism of coating nucleation which is similar to that of CCCs [26–29]. This follows the similar electrochemical nature for deposition in both types of system, even though different pH values are used.

### 3.3. Thicker coating formation

Fig. 4 shows some surface images for samples after PCC growth for 90 and 150 min at 25 °C. In contrast to samples permanganated for shorter times (Fig. 2), no polishing scratches can now be seen, and this is indicative of the surfaces being well covered by PCC when the treatments are for these longer times. The surface of the alloy matrix (Fig. 4c) is fully covered by a relatively uniform and crack-free coating with hillock-like morphology, whereas the particles are coated with PCC that appears dense and featureless (Fig. 4a,b,d). As shown in Fig. 4b, most of the bigger Al–Cu–Fe–Mn second-phase particles demonstrate cracked coating, which could result from the drying of relatively thick films on top of the particles, analogous to observations for thick CCCs [27]. This phenomenon seems less apparent for the Al–Cu–Mg particles. The difference may depend on the particles' nature, or it may follow more from the bigger size and irregular shape for the Al–Cu–Fe–Mn particles. The deep trenches seen around the heavily coated Al–Cu–Mg particles (Fig. 4d) could be caused either by electrochemical dissolution at the adjacent alloy matrix, or by a large difference in PCC thickness between the particles and their surroundings; the former would be most consistent with the experience for CCC formation [27].

The thicker PCCs are too insulating to be probed by Auger point analysis, and therefore their characterization was made by EDX in selective area analysis. Assuming a chemically uniform coating over a second-phase particle, or over the matrix at a

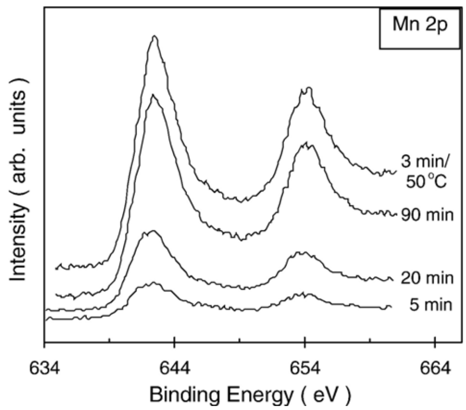


Fig. 5. Mn 2p spectra measured from 2024-Al samples after different PCC treatments. The coating times are indicated; the top curve applies to a treatment at 50 °C while the others are for 25 °C.

particular area, the atomic ratio of Mn in the coating to the sum of all major metals (M = Al, Cu, Mg, Fe, Mn) in the substrate (i.e. $Mn_{coating}/\Sigma M_{substrate}$) should provide a guide to the relative PCC thickness at the region of interest. Since EDX characterizations show that Mn is present in 2024-Al at the same regions and at approximately the same level as Fe, this ratio can be estimated in practice as

$$R = (X_{Mn} - X_{Fe})/(X_{Al} + X_{Cu} + X_{Mg} + 2X_{Fe}), \tag{5}$$

where $X_M$ represents the amount of M (in at%) detected by EDX from a local region. Eq. (5) can thus be applied equally to the Al–Cu–Fe–Mn second-phase particles (with $X_{Mn} \approx X_{Fe}$), as well as the Al–Cu–Mg particles and the matrix (where $X_{Mn} \approx X_{Fe} \approx 0$).

The sample treated for 90 min at 25 °C demonstrated a quite uniform Mn oxide coating over the alloy matrix, with the ratio $R$ equal to about 0.008 from all selected areas (diameter ~ 1 μm). (Incidentally the ratio was also found to be between 0.008 and 0.009 for matrix regions of the sample treated for 3 min at 50 °C, which is consistent with observations from XPS for these two samples.) For comparison, EDX selective area analyses for the particles marked with crosses in Fig. 4a,b gave $R$ values equal to ~ 0.04 and ~ 0.05 respectively (approximately five times greater than $R$ values for the matrix). Thus, it is clear that the Mn oxide deposits are significantly greater over the particles in the sample permanganated for 90 min, and the same statement holds for samples treated for longer times (samples treated for 3 min at 50 or 68 °C also show the same trend).

The alloy matrix for samples permanganated for 150 and 210 min at 25 °C demonstrated $R$ values of ~ 0.009–0.01 for both coating times, indicating that the growth had essentially self-limited by about 150 min, and the same statement holds for coating on the particles. The self-limiting time observed in this work is longer than that reported by Bibber (~ 60 min at 25 °C) [9], and the difference possibly relates to variations in surface pre-treatment prior to immersion in the permanganating bath.

Bibber reported for Al alloys with high Cu or Zn contents that a sealing procedure needs to be applied on a PCC in order to provide adequate protection in a corrosive environment [7–11]. The high cathodic activity of the Cu-containing second-phase particles in 2024-Al results in defects appearing on the surface after the PCC treatment, and this includes cracks in coatings over large particles and peripheral trenches (Fig. 4b,d). That the smaller Al–Cu–Mg particles did not demonstrate observable PCC cracks suggests there is a size dependence as well as a tendency for the defect formation to be associated with the noble character (cathodicity) of alloy inclusions. This work therefore demonstrates ways in which the more noble inclusions in the 2024-Al alloy lead to weaknesses in a prepared PCC, thereby opening the need for further sealing.

### 3.4. Mn oxidation state in coatings

Fig. 5 presents Mn 2p spectra measured from samples PCC-treated at 25 °C for 5, 20 and 90 min, as well as for 3 min at 50 °C. Samples treated at 25 °C for 150 and 210 min, or at 68 °C for 3 min, show XPS spectra consistent with those in Fig. 5, but with somewhat increased intensities. Throughout, two main peaks are apparent, associated with $2p_{3/2}$ and $2p_{1/2}$ at binding energies of about 642.5 and 654.0 eV respectively, although a regular curve fitting is hindered by the asymmetric nature of these peaks. Accordingly we rely on a more qualitative discussion, which notes that the Mn $2p_{3/2}$ peak for $MnO_2$ is expected at around 641.8-642.3 eV [30,31]. This is consistent with measured spectra, earlier reports for PCCs [14,15] and permanganate-phosphate coatings [19] on Mg alloys, and the reaction in Eq. (4), although the coated species may be hydrated to some degree. The Mn $2p_{3/2}$ peak for Mn(III) oxide is expected to be ~0.5 eV less [30,31], while that for Mn(VII) is 3 eV or more greater [30–34]. Therefore it appears from direct observation of the measured spectra in Fig. 5 that any permanganate incorporation into the PCCs must be quite small.

The observation here that there is no appreciable incorporation of permanganate anions into PCCs under the conditions applied differs from reports by Danilidis et al. [6] and Bibber [8] who detected, using infrared spectroscopy, $MnO_4^-$ anions in their PCCs on aluminum alloys. As the ‘no-rinse’ procedure was used by Danilidis et al. [6], it may be that some amount of unreacted permanganate species remained on the sample surface after the coating and annealing at 100 °C; no detailed history of the specimen studied was given by Bibber [8]. That no significant incorporation of Mn(VII) into the growing PCCs occurs in this work may relate to an observation that PCCs do not form ‘inorganic polymers’ combining both the oxidized and reduced species Mn(VII) and Mn(IV) [8]. By contrast, polymeric structures involving Cr(III)-O-Cr(VI) covalent bonding are reported to occur in CCCs [12].

## 4. Conclusions

The initial and further growth of permanganate conversion coatings (PCCs) on 2024-Al alloy has been studied by using a combination of surface analysis and materials analysis techniques. The process is shown to be electrochemical in nature with $MnO_2$ deposition first over the intermetallic second-phase particles driven by their cathodicity with respect to the alloy matrix. The subsequent film nucleation and growth occurs on the Al matrix. The process is slow at room temperature and self-limits after about 150 min. Within the temperature range studied (25–68 °C), comparable film morphologies and coatings were observed, with the PCC process being faster at the higher temperatures.

Al, Cu and B could not be detected by XPS in thicker coatings, but inclusions of Mg, K and Na were recognized at the later growth stages. The mechanism for incorporation of these inclusions during permanganating remains unclear. No significant amount of $MnO_4^-$ entrapped by the growing coatings was detected by XPS, and this may limit the 'self-healing' ability of PCCs compared with CCCs.

The coatings formed over second-phase particles are considerably thicker than over the alloy matrix throughout the range of immersion time investigated at 25 °C. Cracks are observed in thick PCC films covering the larger second-phase particles, but not on the alloy matrix, where the coating is relatively uniform and significantly thinner. These observations of morphology show a difference from the CCCs, since the latter are thicker over the alloy matrix and form cracks over all the surface after drying [27]. Therefore different failure mechanisms in corrosion protection can be expected for PCCs compared with the CCCs.

## Acknowledgement

We are grateful for the support provided for this research by the Natural Sciences and Engineering Research Council of Canada.

## References

[1] H. Guan, R.G. Buchheit, Corrosion 60 (2004) 284.
[2] X. Zhang, C. Van den Bos, W.G. Sloof, A. Hovstad, H. Terryn, J.H.W. de Wit, Surf. Coat. Technol. 199 (2005) 92.
[3] A.N. Khramov, N.N. Voevodin, V.N. Balbyshev, R.A. Mantz, Thin Solid Films 483 (2005) 191.
[4] A. Decroly, J.-P. Petitjean, Surf. Coat. Technol. 194 (2005) 1.
[5] A.S. Akhtar, D. Susac, P. Glaze, K.C. Wong, P.C. Wong, K.A.R. Mitchell, Surf. Coat. Technol. 187 (2004) 208.
[6] I. Danilidis, J.M. Sykes, J.A. Hunter, G.M. Scamans, Surf. Eng. 15 (1999) 401.
[7] J.W. Bibber, Proc. Corrosion 95: The NACE International Annual Conference and Corrosion Show. March 1995, NACE International, Orlando, FL, 1995, (Paper 392).
[8] J.W. Bibber, Plating Surf. Finish. 90 (2003) 40.
[9] J.W. Bibber, U.S. Patent 4,755,224 (1988).
[10] J.W. Bibber, U.S. Patent 4,878,963 (1989).
[11] J.W. Bibber, U.S. Patent 4,988,396 (1991).
[12] L. Xia, R.L. McCreery, J. Electrochem. Soc. 145 (1998) 3083.
[13] M. Takaya, Jpn. Inst. Light Met. 45 (1995) 713 (In Japanese).
[14] H. Umehara, S. Terauchi, M. Takaya, Mater. Sci. Forum 350-351 (2000) 273.
[15] H. Umehara, M. Takaya, S. Terauchi, Surf. Coat. Technol. 169-170 (2003) 666.
[16] C.S. Lin, C.Y. Lee, W.C. Li, Y.S. Chen, G.N. Fang, J. Electrochem. Soc. 153 (2006) B90.
[17] M. Zhao, S.S. Wu, J.R. Luo, Y. Fukuda, H. Nakae, Surf. Coat. Technol. 200 (2006) 5407.
[18] D. Hawke, D.L. Albright, Met. Finish. 93 (10) (1995) 34.
[19] K.Z. Chong, T.S. Shih, Mater. Chem. Phys. 80 (2003) 191.
[20] R.G. Buchheit, M. Cunningham, H. Jensen, M.W. Kendig, M.A. Martinez, Corrosion 54 (1998) 61.
[21] R.G. Buchheit, R.P. Grant, P.F. Hlava, B. Mckenzie, G.L. Zender, J. Electrochem. Soc. 144 (1997) 2621.
[22] J.C. Russ, Fundamentals of Energy Dispersive X-ray Analysis, Butterworths, London, 1984, p. 115.
[23] M. Pourbaix, Atlas of Electrochemical Equilibria in Aqueous Solutions, Pergamon Press, 1966, p. 171.
[24] A. Nylund, Alum. Trans. 2 (2000) 121.
[25] D. Susac, X. Sun, K.A.R. Mitchell, Appl. Surf. Sci. 207 (2003) 40.
[26] G.M. Brown, K. Kobayashi, J. Electrochem. Soc. 148 (2001) B457.
[27] P. Campestrini, H. Terryn, J. Vereecken, J.H.W. de Wit, J. Electrochem. Soc. 151 (2004) B359.
[28] S.A. Kulinich, A.S. Akhtar, D. Susac, K.C. Wong, P.C. Wong, K.A.R. Mitchell, Mater. Sci. Forum 519-521 (2006) 621.
[29] S.A. Kulinich, A.S. Akhtar, D. Susac, P.C. Wong, K.C. Wong, K.A.R. Mitchell, Appl. Surf. Sci. 253 (2007) 3144.
[30] J.F. Moulder, W.F. Stickle, P.E. Sobol, K.D. Bomben, Handbook of X-ray Photoelectron Spectroscopy, Physical Electronics, Eden Prairie, 1995.
[31] A.A. Audi, P.M.A. Sherwood, Surf. Interface Anal. 33 (2002) 274.
[32] Y. Umezawa, C.N. Reilley, Anal. Chem. 50 (1978) 1290.
[33] M. Oku, J. Electron Spectrosc. Relat. Phenom. 74 (1995) 135.
[34] M. Oku, H. Matsuta, K. Wagatsuma, Bunseki Kagaku 46 (1997) 703 (In Japanese).